Journal of Marine Science and Application (2023) 22: 456-474
https://doi.org/10.1007/s11804-023-00346-6

RESEARCH ARTICLE

Wave Energy Damping due to Coupled Porous Structure and Submerged Porous Plate

K.R. Athul Krishna[1], Khansa Abdulla[1] and D. Karmakar[1]

Received: 07 September 2022 / Accepted: 08 January 2023

Abstract
The present study investigates the wave-damping characteristics due to the combination of bottom-standing porous structure, submerged porous plate, and fully-extended porous structure of finite width using the small amplitude wave theory. The hydrodynamic characteristics such as reflection, transmission, and dissipation coefficients are determined to analyse the wave energy dissipation by the composite breakwater using the matched eigenfunction expansion method and orthogonal mode-coupling relation. Darcy's law is incorporated to the flow through porous media. The composite breakwater system is investigated experimentally to validate and compare the numerical results with the physical model study. The complex porous effect parameter for the submerged plate is incorporated in the numerical analysis, which represents the reactance and resistance of the porous structure. The wave forces on the submerged plate and porous structure for the composite breakwater are investigated by considering the effects of changing parameters such as structural porosity, plate submergence, angle of incidence, width of the submerged porous structure and distance between the structures. The study illustrates that the increasing width of the fully-extended porous structure improves the performance of the breakwater system. The proposed study on the composite breakwater yields an useful information for wave energy attenuation, which can be designed and implemented in coastal and harbour areas to achieve wave tranquillity.

Keywords Fully-extended porous structure; Wave transmission; Energy dissipation; Porosity; Submerged horizontal porous plate

1 Introduction

Ports and harbours have become an integral part of a country's economic development, channeling most of its trade and offering a strategic location for naval deployment. A tranquil condition is essential for proper functioning facilities inside the port and harbour, which ensure the safe anchorage of marine vessels. Adequate coastal protection measures are inevitable for the safety of coastal communities. The porous structures are employed in coastal regions for the energy dissipation of gravity waves, thus creating a tranquil zone on the leeward side of the structure. The porous structures also reduces and eliminate the littoral drift, which is one of the main drawbacks of the traditional rubble mound breakwaters. The porous structure offers the advantage of allowing water to pass through the structure, thereby reducing the wave load impact on the structure and enhancing its durability, which is not the case for conventional breakwater. Moreover, the submerged porous structures are simple to construct and do not alter the coast's appealing aesthetic appearance. Further, the maintenance required for porous structures is less when compared to that of traditional breakwaters. A significant studies on wave interaction with porous structures is performed by Dick and Brebner (1968), Dattatri et al. (1978), Madsen (1983), Sulisz (1985), Dalrymple et al. (1991), Losada et al. (1991, 1995, 1996), Huang and Chao (1992) and Ting et al. (2004). The study illustrates that the the submerged porous structure is effective in the dissipation of wave energy and has pooved to be an efficient breakwater for the protection of coastal facilities.

Article Highlights

- The hydrodynamic performance of composite breakwater consisting of porous structure and submerged plate is analysed analytically and validated using the experimental investigation.
- The effect of structural and geometrical parameters are analysed for the compsite breakwater system.
- The influence of the wave attenuation charecteristics along with wave force experience on the composite breakwater sustem is analysed.

✉ D. Karmakar
dkarmakar@nitk.edu.in

[1] Department of Water Resources and Ocean Engineering, National Institute of Technology Karnataka, Surathkal, Mangalore-575025, India

Researchers have performed commendable studies on the breakwaters with different cross-sections and the submerged bottom-standing porous structures are highly capable of dissipating wave energy without causing any hindrance to the shoreward flow of water. Bennett et al. (1992) proposed a theory for interacting an incident plane wave with a slotted wave-screen breakwater. The study suggests a semi-empirical nonlinear term containing a head-loss coefficient that accounts for the impacts of energy dissipation in the flow through the screen. Zhu and Chwang (2001) performed an analytical study on the wave reflection characteristics due to composite porous breakwater lying on a solid foundation having a seaward slope. The study observed that the presence of a solid foundation does not have much effect on the reflection characteristics. The wave trapping by bottom standing and surface piecing porous structures backed by a rigid wall is examined by Koley et al. (2015). The wave reflection due to the surface-piercing porous structure is small compared to the bottom-standing porous structure. Somervell et al. (2018) derived an empirical formula for determining the friction coefficient of a double-walled permeable vertical breakwater consisting of two perforated walls spaced at a certain distance. Recently, Li et al. (2021) developed a new analytical solution for the oblique wave scattering by a perforated structure presenting the matrix element into a new form using the contour integral technique.

The studies on submerged horizontal porous plate proved to achieve wave attenuation and also helps in reducing the problem of littoral transport as they permit easy flow of water. The experimental study conducted by Neelamani and Reddy (1992) on the wave hydrodynamic characteristics of a rigidly fixed surface and submerged horizontal plate showed that the transmission coefficient is minimum and the reflection coefficient is maximum when the plate is at still water level. Neelamani and Gayathri (2006) experimentally studied the performance of a twin-plate wave barrier for different wave heights and wave periods and observed that the transmission coefficient reduces and the reflection coefficient increases as the relative width of the plate increase. Liu and Li (2011) formulated an alternative analytical solution for water motion over an offshore horizontal plate breakwater and found that the results were similar with the results obtained by other analytical approaches. Cho and Kim (2013) studied the interaction of incident waves with a submerged horizontal breakwater which showed that the wave-structure interaction enhances as plate width increases. Cho et al. (2013) conducted an experimental study on the dual porous submerged horizontal breakwater. The study found no significant variation in the performance of the proposed structure when the lower porous plate is added at a gap greater than 10% of water depth. Das and Bora (2014) studied the reflection of oblique gravity waves by a rectangular porous structure placed on an elevated horizontal impermeable bottom supported by a solid vertical wall at one end. The results are compared with that of horizontal ocean bottom (without any elevation) to examine the effect of the elevated bottom. Recently, Mohapatra et al. (2018) presented an analytical study on the interaction of gravity waves with submerged flexible horizontal plates, suggesting wave attenuation depends on mooring stiffness and porous effect parameter.

Multiple porous structures have proved to be more effective than single porous structures. These structures can be either vertically or horizontally stratified or a series of structures placed at certain distances. Twu and Chieu (2000) developed an offshore breakwater composed of multiple layers of porous structures with different porosities with low values of reflection and transmission coefficients. Twu et al. (2002) studied the wave energy dissipation characteristics of vertically stratified porous structure under wave attack. The wave damping is noted to increase as the porosity and thickness of structures increases. Yang et al. (2017) studied the performance of multiple submerged porous bars near a vertical wall under wave attack using an analytical solution. The study observed that the spacing between the bars should be appropriately determined for better performance. The performance of stratified porous blocks backed by a sea wall due to the presence of flat, elevated, and stepped sea beds are studied by Venkateswarlu and Karmakar (2020). The reduction in wave force on the sea wall in the case of a stepped bed is noted when compared to a flat and elevated bed. Further, Venkateswarlu and Karmakar (2021) performed a numerical analysis on the wave-dissipating characteristics of multiple porous structures of finite thickness considering the leeward unbounded region and confined region, which suggested that the increase in the number of structures enhances wave damping.

Studies on floating-type breakwaters have been of broad interest over the years. These breakwaters are economical when there is a need to provide a calm sheltered region for a short duration as these are mobile structures that can be transported after their use, unlike the conventional breakwaters. Arunachalam (1982) conducted experimental studies on porous horizontal floating plate breakwater and found that the transmission characteristics are greatly influenced by the wave steepness and length of the breakwater. Wang and Sun (2010) experimentally studied the performance of a porous floating breakwater under waves. The study observed that the transmission reduces with increased lengths of the breakwater and the mooring force. Patil and Karmakar (2022) analysed the hydrodynamic characteristics of a floating tunnel with submerged rubble mound breakwater (SRMB). The hydrodynamic coefficient are observed to be efficient with the increased depth of submer-

gence for increased porosity in the SRMB armour layer. Xie (2022) analysed long wave reflection from an array of trapezoidal breakwaters. The sloping seabed is noted to surpass the resonance frequency while strengthening the Bragg reflection.

The studies performed by researchers provided limited information regarding the wave-damping characteristics of combinations of different types of porous structures. Hence, to bridge the research gap, the present study analyses the wave dissipation characteristics of various combinations of bottom-standing porous structures, submerged horizontal porous plate, and fully extended porous structures. The matched eigenfunction expansion method and the orthogonal mode-coupling relation are incorporated to determine the wave transformation along with the wave force due to the composite breakwater system. The study provides insight into the optimum configuration for which the porous structure achieves maximum wave energy dissipation, enhancing the efficiency of the coastal structure.

2 Mathematical formulation for composite breakwater

The wave interaction with a combination of bottom-standing porous structure, submerged porous plate, and the fully-extended porous structure is analysed using the small-amplitude wave theory. The Cartesian coordinate system is considered with x-axis taken as horizontal and the y-axis considered vertically downward positive. The fluid domain is divided into nine regions (Figure 1), upstream open water region at $0 < x < \infty, 0 < y < h$ as region-1 (R_1), the fluid domain above the bottom-standing porous structure at $-a_1 < x < 0, 0 < y < h_1$ is taken as region-2 (R_2), bottom-standing submerged porous structure region at $-a_1 < x < 0, h_1 < y < h$ is taken as region-3 (R_3), fluid domain between the porous structure and porous plate at $-a_2 < x <- a_1, 0 < y < h$ as region-4 (R_4), fluid domain above the porous plate at $-a_3 < x < -a_2, 0 < y < h_1$ as region-5 (R_5), fluid domain below the submerged porous plate at $-a_3 < x <- a_2, h_1 < y < h$ as region-6 (R_6), fluid domain between the plate and the fully extended porous structure at $-a_4 < x <- a_3, 0 < y < h$ as region-7 (R_7), fully-extended porous structure at $-a_5 < x <- a_4, 0 < y < h$ as region-8 (R_8) and downstream open water region at $-\infty < x <- a_5, 0 < y < h$ as region-9 (R_9).

The fluid is a considered to be incompressible, inviscid and the motion is irrotational and simple harmonic in time with frequency ω and the velocity potential $\Phi_j(x, y, z, t)$ in the respective regions are represented as $\Phi_j(x, y, z, t) = \mathrm{Re}\left\{\phi_j(x, y)\mathrm{e}^{-\mathrm{i}lz - \mathrm{i}\omega t}\right\}$ along with the free surface deflection represented as $\zeta_j(x, z, t) = \mathrm{Re}\left\{\eta_j(x)\mathrm{e}^{-\mathrm{i}lz - \mathrm{i}\omega t}\right\}$ where Re is the real part and $l = \gamma_{10}\sin\theta$ is the wavenumber in z direction, θ is the angle of incidence, γ_{10} is the progressive wave number in y direction and the subscript j denotes the respective regions. The velocity potential $\phi_j(x, y)$ satisfies the Helmholtz equation given by

$$\frac{\partial^2\phi_j}{\partial x^2} + \frac{\partial^2\phi_j}{\partial y^2} - l^2\phi_j = 0 \quad \text{for } 0 < y < h \tag{1}$$

The bottom is considered to be impermeable without any elevation, and there is no flow of fluid through the sea bed. So the bottom boundary condition is of the form

$$\frac{\partial\phi_j(x, y)}{\partial y} = 0 \text{ at } y = h \text{ for } j = 1, 4, 6, 7, 9 \tag{2}$$

The linearized free surface boundary condition in open water region is given by

$$\frac{\partial\phi_j(x, y)}{\partial y} + \frac{\omega^2}{g}\phi_j(x, y) = 0 \text{ at } y = 0 \text{ for } j = 1, 4, 7, 9 \tag{3}$$

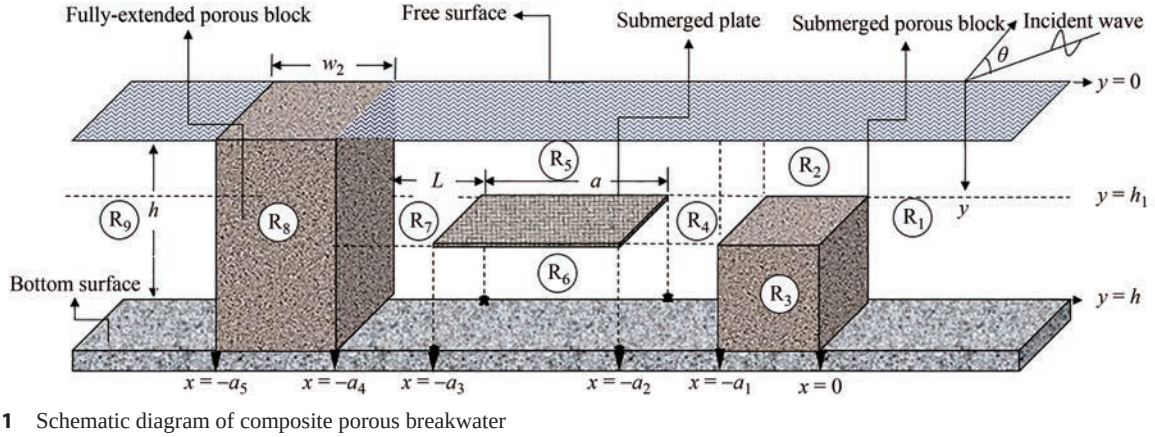

Figure 1 Schematic diagram of composite porous breakwater

The linearized free surface condition in the porous structure region for the bottom-standing porous structure is given by

$$\frac{\partial \phi_j(x,y)}{\partial y} + \frac{\omega^2(s_1 + \mathrm{i}f_1)}{g}\phi_j(x,y) = 0 \quad \text{at} \quad h1 < y < h \quad \text{for} \quad j = 3 \tag{4a}$$

where s_1 is the inertia coefficient and f_1 is the friction coefficient for the bottom-standing porous structure. The linearized boundary condition for the porous plate at the interface is given by

$$\frac{\partial \phi_5}{\partial y} = \frac{\partial \phi_6}{\partial y} = \mathrm{i}\gamma_{10} G_p(\phi_6 - \phi_5) \quad \text{for} \quad y = h_1 \tag{4b}$$

where $G_p = \dfrac{\rho b \omega}{\mu}$ is the porous effect parameter, ρ is the density of the structure, b is the material constant and μ is the dynamic viscosity constant. Further, the linearized boundary condition for the fully-extended porous structure is given by

$$\frac{\partial \phi_j(x,y)}{\partial y} + \frac{\omega^2(s_2 + \mathrm{i}f_2)}{g}\phi_j(x,y) = 0 \quad \text{at} \quad y = 0 \quad \text{for} \quad j = 8 \tag{4c}$$

where s_2 is the inertia coefficient and f_2 is the friction coefficient of the fully-extended porous structure. The boundary condition at the interface $y = h_1$ for the bottom-standing porous structure is given by

$$\phi_2 = (s_1 + \mathrm{i}f_1)\phi_3 \quad \text{and} \quad \frac{\partial \phi_2}{\partial y} = \varepsilon_1 \frac{\partial \phi_3}{\partial y} \tag{5}$$

The continuity of velocity and pressure at the edge $x = 0, -a_1$ is given by

$$\phi_2(x,y) = \begin{cases} \phi_1(x,y)\big|_{x=0} \\ \phi_4(x,y)\big|_{x=-a_1} \end{cases} \text{ and } \phi_{2x}(x,y) = \begin{cases} \phi_{1x}(x,y)\big|_{x=0} \\ \phi_{4x}(x,y)\big|_{x=-a_1} \end{cases} \text{ for } 0 < y < h_1 \tag{6a}$$

$$(s_1 + \mathrm{i}f_1)\phi_3(x,y) = \begin{cases} \phi_1(x,y)\big|_{x=0} \\ \phi_4(x,y)\big|_{x=-a_1} \end{cases} \text{ and } \varepsilon_1\phi_{3x}(x,y) = \begin{cases} \phi_{1x}(x,y)\big|_{x=0} \\ \phi_{4x}(x,y)\big|_{x=-a_1} \end{cases} \text{ for } h_1 < y < h \tag{6b}$$

Further, at the edge $x = -a_j, j = 2, 3$ of the fluid and porous plate interfaces, the continuity of velocity and pressure is given by

$$\phi_5(x,y) = \begin{cases} \phi_4(x,y)\big|_{x=-a_2} \\ \phi_7(x,y)\big|_{x=-a_3} \end{cases} \text{ and } \phi_{5x}(x,y) = \begin{cases} \phi_{4x}(x,y)\big|_{x=-a_2} \\ \phi_{7x}(x,y)\big|_{x=-a_3} \end{cases} \text{ for } 0 < y < h_1 \tag{7a}$$

$$\phi_6(x,y) = \begin{cases} \phi_4(x,y)\big|_{x=-a_2} \\ \phi_7(x,y)\big|_{x=-a_3} \end{cases} \text{ and } \phi_{6x}(x,y) = \begin{cases} \phi_{4x}(x,y)\big|_{x=-a_2} \\ \phi_{7x}(x,y)\big|_{x=-a_3} \end{cases} \text{ for } h_1 < y < h \tag{7b}$$

In addition, at the edge $x = -a_j, j = 4, 5$ of the fully-extended porous structure, the continuity of velocity and pressure is given by

$$(s_2 + \mathrm{i}f_2)\phi_8(x,y) = \begin{cases} \phi_7(x,y)\big|_{x=-a_4} \\ \phi_9(x,y)\big|_{x=-a_5} \end{cases} \text{ and } \varepsilon_2\phi_{8x}(x,y) = \begin{cases} \phi_{7x}(x,y)\big|_{x=-a_4} \\ \phi_{9x}(x,y)\big|_{x=-a_5} \end{cases} \text{ for } 0 < y < h \tag{8}$$

The wave number in the upstream/downstream free-water region γ_{jn} for $j = 1, 4, 7, 9$ and the bottom-standing porous structure region γ_{2n} satisfies the dispersion relation for finite water depth is given by

$$\omega^2 = \begin{cases} g\gamma_{j0}\tanh\gamma_{j0}h & \text{for} \quad n = 0 \\ -g\gamma_{jn}\tan\gamma_{jn}h & \text{for} \quad n = 1, 2, ... \end{cases} \text{for} \quad j = 1, 4, 7, 9 \tag{9a}$$

$$\omega^2 - g\gamma_{2n}\tanh\gamma_{2n}h - F_n(\omega^2\tanh\gamma_{2n}h - \gamma_{2n}g) = 0 \quad \text{for} \quad n = 0, 1, 2, ... \tag{9b}$$

where $F_n = \dfrac{\{(s_1 + \mathrm{i}f_1) - \varepsilon_1\}\tanh\gamma_{2n}(h - h_1)}{\{(s_1 + \mathrm{i}f_1) - \varepsilon_1\tanh^2\gamma_{2n}(h - h_1)\}}$, ω is the wave frequency and g is the acceleration due to gravity. Further, the wave number γ_{5n} within $-a_2 < x < -a_3, 0 < y < h$ satisfies the dispersion relation of the form for $n = 0, 1, 2, ...$ given by

$$\gamma_{5n}\sinh\gamma_{5n}(h - h_1)\{g\gamma_{5n}\sinh\gamma_{5n}h_1 - \omega^2\cosh\gamma_{5n}h_1\} - \mathrm{i}k_{10}G_p\{\omega^2\cosh\gamma_{5n}h - g\gamma_{5n}\sinh\gamma_{5n}h\} = 0 \tag{10}$$

The wave number γ_{8n} for the fully-extended porous structure satisfies the dispersion relation given by

$$\omega^2(s_2 + \mathrm{i}f_2) = g\gamma_{8n}\tanh\gamma_{8n}h \quad \text{for} \quad n = 0, 1, 2, ... \tag{11}$$

In the far-field region, the radiation conditions in the presence of a porous structure with the barrier are given by

$$\phi_j(x,y) = \begin{cases} \left(I_{10}e^{-iy_{10}x} + R_{10}e^{iy_{10}x}\right) f_{10}(y) & \text{as } x \to \infty \\ \left(T_{90}e^{-iy_{90}x}\right) f_{90}(y) & \text{as } x \to -\infty \end{cases} \quad (12)$$

where I_{10}, R_{10} and T_{90} are the complex amplitude of the incident, reflected and transmitted wave amplitudes respectively.

3 Method of solution for composite breakwater

The velocity potentials $\phi_j(x,y)$ in each of the regions satisfy the Helmholtz Equation (1) along with the boundary conditions (2) – (4) is of the form

$$\phi_1(x,y) = (I_{10}e^{-ik_{10}x} + R_{10}e^{ik_{10}x}) f_{10}(y) + \sum_{n=1}^{\infty} R_{1n}e^{-k_{1n}x} f_{1n}(y) \text{ for } 0 < x < \infty, 0 < y < h \quad (13a)$$

$$\phi_2(x,y) = \sum_{n=0}^{\infty} \left\{A_{2n}e^{-ik_{2n}x} + B_{2n}e^{ik_{2n}(x+a_1)}\right\} f_{2n}(y) \text{ for } -a_1 < x < 0, 0 < y < h_1 \quad (13b)$$

$$\phi_3(x,y) = \sum_{n=0}^{\infty} \left\{A_{2n}e^{-ik_{2n}x} + B_{2n}e^{ik_{2n}(x+a_1)}\right\} f_{3n}(y) \text{ for } -a_1 < x < 0, h_1 < y < h \quad (13c)$$

$$\phi_4(x,y) = (A_{40}e^{-ik_{40}(x+a_1)} + B_{40}e^{ik_{40}(x+a_2)}) f_{40}(y) + \sum_{n=1}^{\infty} \left\{A_{4n}e^{k_{4n}(x+a_1)} + B_{4n}e^{-k_{4n}(x+a_2)}\right\} f_{4n}(y) \text{ for } -a_2 < x <- a_1, 0 < y < h \quad (13d)$$

$$\phi_5(x,y) = \sum_{n=0}^{\infty} \left\{A_{5n}\frac{\cos k_{5n}x}{\cos k_{5n}a_2} + B_{5n}\frac{\sin k_{5n}x}{\sin k_{5n}a_3}\right\} f_{5n}(y) \text{ for } -a_3 < x <- a_2, 0 < y < h_1 \quad (13e)$$

$$\phi_6(x,y) = \sum_{n=0}^{\infty} \left\{A_{5n}\frac{\cos k_{5n}x}{\cos k_{5n}a_2} + B_{5n}\frac{\sin k_{5n}x}{\sin k_{5n}a_3}\right\} f_{6n}(y) \text{ for } -a_3 < x <- a_2, h_1 < y < h \quad (13f)$$

$$\phi_7(x,y) = (A_{70}e^{-ik_{70}(x+a_3)} + B_{70}e^{ik_{70}(x+a_4)}) f_{70}(y) + \sum_{n=1}^{\infty} \left\{A_{7n}e^{k_{7n}(x+a_3)} + B_{7n}e^{-k_{7n}(x+a_4)}\right\} f_{7n}(y) \text{ for } -a_4 < x <- a_3, 0 < y < h \quad (13g)$$

$$\phi_8(x,y) = \sum_{n=0}^{\infty} \left\{A_{8n}e^{-ik_{8n}(x+a_4)} + B_{8n}e^{ik_{8n}(x+a_5)}\right\} f_{8n}(y) \text{ for } -a_5 < x <-a_4, 0 < y < h \quad (13h)$$

$$\phi_9(x,y) = T_{90}e^{-ik_{90}(x+a_5)} f_{90}(y) + \sum_{n=1}^{\infty} T_{9n}e^{k_{9n}(x+a_5)} f_{9n}(y) \text{ for } -\infty < x <-a_5, 0 < y < h \quad (13i)$$

where I_{10} is the incident wave amplitude taken as unity and $R_{1n}, A_{2n}, B_{2n}, A_{4n}, B_{4n}, A_{5n}, B_{5n}, A_{7n}, B_{7n}, A_{8n}, B_{8n}$ and T_{9n} for $n = 0, 1, 2, ...$ the unknown constants are to be determined. The eigenfunctions for the open-water regions for $j = 1, 4, 7, 9$ are given by

$$f_{jn}(y) = \frac{\cosh\gamma_{jn}(h-y)}{\cosh\gamma_{jn}h} \text{ for } n = 0 \text{ and } f_{jn}(y) = \frac{\cos\gamma_{jn}(h-y)}{\cos\gamma_{jn}h} \text{ for } n = 1, 2, 3, ... \quad (14)$$

where γ_{jn} for $j = 1, 4, 7, 9$ are the eigenvalues and will satisfy the open water dispersion relation as in Eq. 9(a) satisfying ${\gamma_{jn}}^2 = {k_{jn}}^2 + l^2$, where γ_{jn} is the wave number in y direction, k_{jn} is the wave number in x direction, and $l = \gamma_{10}\sin\theta$ is the wave number in the z direction. The eigenfunctions $f_{jn}(y)$ for $j = 2, 3$ for the bottom-standing submerged porous structure region are given by

$$f_{2n}(y) = \left\{\frac{\cosh\gamma_{2n}(h-y) - F_n\sinh\gamma_{2n}(h-y)}{\cosh\gamma_{2n}h - F_n\sinh\gamma_{2n}h}\right\} \quad (15)$$

$$f_{3n}(y) = \left\{\frac{1 - F_n\tanh\gamma_{2n}(h-h_1)}{(s_1 + if_1)(\cosh\gamma_{2n}h - F_n\sinh\gamma_{2n}h)}\right\}\cosh\gamma_{2n}(h-y) \quad (16)$$

where $F_n = \dfrac{\{(s_1 + if_1) - \varepsilon_1\}\tanh\gamma_{2n}(h-h_1)}{\{(s_1 + if_1) - \varepsilon_1\tanh^2\gamma_{2n}(h-h_1)\}}$ (17)

ε_1 is the porosity, s_1 is an inertial parameter, and f_1 is the friction coefficient of the bottom-standing porous structure, where γ_{2n} satisfies the dispersion relation as in Eq. (9b). The eigenfunctions for the submerged porous plate region $j = 5$ and 6 is given by

$$f_{5n}(y) = \sinh\gamma_{5n}(h-h_1)\left\{g\gamma_{5n}\cosh\gamma_{5n}y - \omega^2\sinh\gamma_{5n}y\right\} \quad (18a)$$

$$f_{6n}(y) = -\left\{g\gamma_{5n}\sinh\gamma_{5n}h_1 - \omega^2\cosh\gamma_{5n}h_1\right\}\cosh\gamma_{5n}(h-y) \quad (18b)$$

where γ_{5n} is the eigenvalue satisfies the dispersion relation as in Eq. (10). Further, the eigenfunctions $f_{jn}(y)$ for the fully-extended porous structure region at $j = 8$ is given by

$$f_{8n}(y) = \frac{\cosh\gamma_{8n}(h-y)}{\cosh\gamma_{8n}h} \text{ for } n = 0, 1, 2, ... \quad (19)$$

where γ_{8n}, $n = 0, 1, 2, ...$ are eigenvalues and satisfies the dispersion relation as in Eq. (11). The eigenfunction $f_{jn}(y)$ in the open water region $j = 1, 4, 7, 9$ satisfy the orthogonality relation given by

$$\left\langle f_{jm}, f_{jn}\right\rangle_{j=1,4,7,9} = \begin{cases} 0 & \text{for } m \neq n \\ C_n & \text{for } m = n \end{cases} \quad (20)$$

with respect to the orthogonal mode-coupling relation defined by

$$\left\langle f_{jm}, f_{jn}\right\rangle_{j=1,4,7,9} = \int_0^h f_{jm}(y)\, f_{jn}(y)\,\mathrm{d}y \quad (21)$$

where $C_n = \left\{\frac{2\gamma_{jn}h + \sinh 2\gamma_{jn}h}{4\gamma_{jn}\cosh^2\gamma_{jn}h}\right\}$ for $n = 0$ with C_n for $n = 1, 2, 3, ...$ are obtained by substituting $\gamma_{jn} = \mathrm{i}\gamma_{jn}$.

In order to determine the unknown coefficients, the orthogonal mode coupling relation as in Eq. (21) is employed on $\phi_j(x,y)$ and $\phi_{jx}(x,y)$ with the eigenfunction $f_{jm}(y)$ along with continuity of velocity and pressure as in Eq. (6a) across the vertical interface $x = 0$, $0 < y < h$ to obtain

$$\left\langle \phi_j(x,y), f_{jm}(y)\right\rangle_{j=1} = \int_0^h \phi_j(x,y)\, f_{jm}(y)\,\mathrm{d}y$$
$$= \int_0^{h_1} \phi_{j+1}(x,y)\, f_{jm}(y)\,\mathrm{d}y + \quad (22a)$$
$$(s_1 + \mathrm{i}f_1)\int_{h_1}^h \phi_{j+2}(x,y)\, f_{jm}(y)\,\mathrm{d}y \text{ for } m = 0, 1, 2, ...$$

$$\left\langle \phi_{jx}(x,y), f_{jm}(y)\right\rangle_{j=1} = \int_0^h \phi_{jx}(x,y)\, f_{jm}(y)\,\mathrm{d}y$$
$$= \int_0^{h_1} \phi_{(j+1)x}(x,y)\, f_{jm}(y)\,\mathrm{d}y + \quad (22b)$$
$$\varepsilon_1\int_{h_1}^h \phi_{(j+2)x}(x,y)\, f_{jm}(y)\,\mathrm{d}y \text{ for } m = 0, 1, 2, ...$$

Further, the orthogonal mode coupling relation as in Eq. (21) is employed on $\phi_j(x,y)$ and $\phi_{jx}(x,y)$ with the eigenfunction $f_{jm}(y)$ along with continuity of velocity and pressure as in Eq. (6b) across the vertical interface $x = -a_1$, $0 < y < h$ to obtain

$$\left\langle \phi_j(x,y), f_{jm}(y)\right\rangle_{j=4} = \int_0^h \phi_j(x,y)\, f_{jm}(y)\,\mathrm{d}y$$
$$= \int_0^{h_1} \phi_{j-2}(x,y)\, f_{jm}(y)\,\mathrm{d}y + \quad (23a)$$
$$(s_1 + \mathrm{i}f_1)\int_{h_1}^h \phi_{j-1}(x,y)\, f_{jm}(y)\,\mathrm{d}y \text{ for } m = 0, 1, 2, ...$$

$$\left\langle \phi_{jx}(x,y), f_{jm}(y)\right\rangle_{j=4} = \int_0^h \phi_{jx}(x,y)\, f_{jm}(y)\,\mathrm{d}y$$
$$= \int_0^{h_1} \phi_{(j-2)x}(x,y)\, f_{jm}(y)\,\mathrm{d}y + \quad (23b)$$
$$\varepsilon_1\int_{h_1}^h \phi_{(j-1)x}(x,y)\, f_{jm}(y)\,\mathrm{d}y \text{ for } m = 0, 1, 2, ...$$

Now, due to the presence of the submerged floating plate, the orthogonal mode coupling relation as in Eq. (21) is employed on $\phi_j(x,y)$ and $\phi_{jx}(x,y)$ with the eigenfunction $f_{jm}(y)$ along with continuity of velocity and pressure as in Eq. (7a) across the vertical interface $x = -a_2$, $0 < y < h$ to obtain

$$\left\langle \phi_j(x,y), f_{jm}(y)\right\rangle_{j=4} = \int_0^h \phi_j(x,y)\, f_{jm}(y)\,\mathrm{d}y$$
$$= \int_0^{h_1} \phi_{j+1}(x,y)\, f_{jm}(y)\,\mathrm{d}y + \quad (24a)$$
$$\int_{h_1}^h \phi_{j+2}(x,y)\, f_{jm}(y)\,\mathrm{d}y \text{ for } m = 0, 1, 2, ...$$

$$\left\langle \phi_{jx}(x,y), f_{jm}(y)\right\rangle_{j=4} = \int_0^h \phi_{jx}(x,y)\, f_{jm}(y)\,\mathrm{d}y$$
$$= \int_0^{h_1} \phi_{(j+1)x}(x,y)\, f_{jm}(y)\,\mathrm{d}y + \quad (24b)$$
$$\int_{h_1}^h \phi_{(j+2)x}(x,y)\, f_{jm}(y)\,\mathrm{d}y \text{ for } m = 0, 1, 2, ...$$

Further, the orthogonal mode coupling relation as in Eq. (21) is employed on $\phi_j(x,y)$ and $\phi_{jx}(x,y)$ with the eigenfunction $f_{jm}(y)$ along with continuity of velocity and pressure as in Eq. (7b) across the vertical interface $x = -a_3$, $0 <$

$y < h$ to obtain

$$\left\langle \phi_j(x,y), f_{jm}(y) \right\rangle_{j=7} = \int_0^h \phi_j(x,y)\, f_{jm}(y)\,\mathrm{d}y = \int_0^{h_1} \phi_{j-2}(x,y)\, f_{jm}(y)\,\mathrm{d}y + \int_{h_1}^h \phi_{j-1}(x,y)\, f_{jm}(y)\,\mathrm{d}y \text{ for } m = 0, 1, 2, \ldots \tag{25a}$$

$$\left\langle \phi_{jx}(x,y), f_{jm}(y) \right\rangle_{j=7} = \int_0^h \phi_{jx}(x,y)\, f_{jm}(y)\,\mathrm{d}y = \int_0^{h_1} \phi_{(j-2)x}(x,y)\, f_{jm}(y)\,\mathrm{d}y + \int_{h_1}^h \phi_{(j-1)x}(x,y)\, f_{jm}(y)\,\mathrm{d}y \text{ for } m = 0, 1, 2, \ldots \tag{25b}$$

Again, due to the presence of a fully-extended porous structure, the orthogonal mode coupling relation as in Eq. (21) is employed on $\phi_j(x,y)$ and $\phi_{jx}(x,y)$ with the eigenfunction $f_{jm}(y)$ along with continuity of velocity and pressure as in Eq. (8) across the vertical interface $x = -a_4$, $0 < y < h$ to obtain

$$\left\langle \phi_j(x,y), f_{jm}(y) \right\rangle_{j=7} = \int_0^h \phi_j(x,y)\, f_{jm}(y)\,\mathrm{d}y = (s_2 + \mathrm{i}f_2) \int_0^h \phi_{j+1}(x,y)\, f_{jm}(y)\,\mathrm{d}y \text{ for } m = 0, 1, 2, \ldots \tag{26a}$$

$$\left\langle \phi_{jx}(x,y), f_{jm}(y) \right\rangle_{j=7} = \int_0^h \phi_{jx}(x,y)\, f_{jm}(y)\,\mathrm{d}y = \varepsilon_2 \int_0^h \phi_{(j+1)x}(x,y)\, f_{jm}(y)\,\mathrm{d}y \text{ for } m = 0, 1, 2, \ldots \tag{26b}$$

Further, the orthogonal mode coupling relation as in Eq. (21) is employed on $\phi_j(x,y)$ and $\phi_{jx}(x,y)$ with the eigenfunction $f_{jm}(y)$ along with continuity of velocity and pressure as in Eq. (8) across the vertical interface $x = -a_5$, $0 < y < h$ to obtain

$$\left\langle \phi_j(x,y), f_{jm}(y) \right\rangle_{j=9} = \int_0^h \phi_j(x,y)\, f_{jm}(y)\,\mathrm{d}y = (s_2 + \mathrm{i}f_2) \int_0^h \phi_{j-1}(x,y)\, f_{jm}(y)\,\mathrm{d}y \text{ for } m = 0, 1, 2, \ldots \tag{27a}$$

$$\left\langle \phi_{jx}(x,y), f_{jm}(y) \right\rangle_{j=9} = \int_0^h \phi_{jx}(x,y)\, f_{jm}(y)\,\mathrm{d}y = \varepsilon_2 \int_0^h \phi_{(j-1)x}(x,y)\, f_{jm}(y)\,\mathrm{d}y \text{ for } m = 0, 1, 2, \ldots \tag{27b}$$

The infinite sums presented in Eqs. (22)–(27) is truncated up to finite M terms to obtain a linear system of $12(M + 1)$ algebraic equations for the determination of $12(M + 1)$ unknowns, and the wave reflection and transmission due to the combined bottom-standing porous structure, submerged plate and fully-extended porous structure are obtained as

$$K_r = \left| \frac{R_{10}}{I_{10}} \right| \text{ and } K_t = \left| \frac{T_{90}}{I_{10}} \right| \tag{28a}$$

Due to the existence of porous blocks, the energy dissipation in the wave propagation through the porous structure is represented as

$$K_d = 1 - K_r^2 - K_t^2 \tag{28b}$$

The wave force acting on the front and back side of the bottom-standing porous structure can be represented as

$$K_{\mathrm{fs}_1}^1 = \frac{F_f^1}{2\rho g I_{10} h} \text{ and } K_{\mathrm{fs}_2}^1 = \frac{F_b^1}{2\rho g I_{10} h} \tag{29a}$$

where $F_f^1 = \mathrm{i}\rho\omega \int_{h_1}^h (\phi_3 - \phi_1)\mathrm{d}y$ at $x = 0$ (29b)

$$F_b^1 = \mathrm{i}\rho\omega \int_{h_1}^h (\phi_3 - \phi_4)\mathrm{d}y \text{ at } x = -a_1 \tag{29c}$$

The wave force acting on the horizontal porous plate is given by

$$K_p = \frac{F_p}{2\rho g I_{10} h} \tag{30a}$$

where

$$F_p = \mathrm{i}\rho\omega \int_{-a_3}^{-a_2} (\phi_5 - \phi_6)\mathrm{d}x \tag{30b}$$

The wave force acting on the front and back side of fully-extended porous structure can be represented as

$$K_{\mathrm{fs}_1}^2 = \frac{F_f^2}{2\rho g I_{10} h} \text{ and } K_{\mathrm{fs}_2}^2 = \frac{F_b^2}{2\rho g I_{10} h} \tag{31a}$$

where $F_f^2 = \mathrm{i}\rho\omega \int_0^h (\phi_8 - \phi_7)\mathrm{d}y$ at $x = -a_4$ (31b)

$$F_b^2 = \mathrm{i}\rho\omega \int_0^h (\phi_8 - \phi_9)\mathrm{d}y \text{ at } x = -a_5 \tag{31c}$$

4 Physical modelling of composite breakwater

The experimental investigation on the wave interaction with the composite breakwater is carried out in a two-dimensional monochromatic wave flume in the Marine Structures Laboratory of the Department of Water

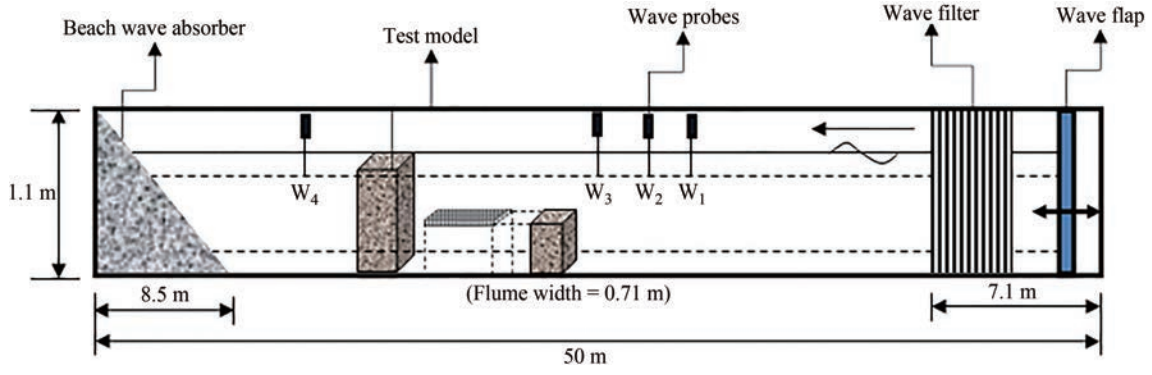

Figure 2 Schematic representation of experimental setup

Resources and Ocean Engineering at the National Institute of Technology Karnataka, India. The total length of the flume is 50 m, with the width and depth being 0.71 m and height of 1.1 m, respectively.

The flume has a channel length of 42 m with a bottom hinged flap-type wave generator at one end and a rubble mound spending beach of slope 1V:10H. The bottom hinged flap-type wave generator is operated by an induction motor (11 kW, 1 450 r/m). The motor is regulated using an inverter drive with a frequency ranging 0 – 50 Hz and rotates at a varying speed of 0 – 155 r/m. The wave filters made of asbestos cement sheet are provided to eliminate the disturbance due to consecutive reflections and to polarize the waves the wave maker generates. The schematic representation of the experimental setup is presented in Figure 2 and the flume details is discussed in Table 1.

Table 1 Flume details

Total length (m)	50
Channel length (m)	42
Width (m)	0.74
Channel depth (m)	1.1
Maximum water depth (m)	0.5
Wave flume type	Two dimensional
Wave Generator	Bottom hinged flap type
Waves generated	Monochromatic type
Wave absorber	Rubble mound spending beach
Range of wave height generation (m)	0.06 – 0.24
Range of wave period generation (s)	1.0 – 3.0

4.1 Model scale

The fundamental of all physical modelling is similitude of the model and prototype. The surface tension and the viscous effects are negligible in the prototype, as in the real sea condition the flow will be turbulent. Also, in wave motion the gravity effect is predominant in the prototype. In such conditions Froude similitude is selected. The choice of scale, for the model test is often limited by constraints posed in the available experimental facility. In the present study, similitude is achieved by the method of dimensional analysis. To simulate the field conditions of wave height, period and depth of water by application of Froude's law, a geometrically similar model scale of 1:30 is selected for the present experimental work.

The breakwater model is tested with the existing facilities in Wave Flume laboratory of Department of Water Resources and Ocean Engineering, NITK, Surathkal. The wave height and wave period of Mangalore coast varies from 1–5.4 m, 8–12 s respectively. In the laboratory regular wave height ranges from 0.06–0.24 m and wave period ranging from 1–3 s can be generated in a maximum water depth of 0.70 m. So, for the studies, a geometrically similar scale (Table 2) of 1:30 is selected for the present experimental investigation.

Table 2 Selection of the model scale

Scale	H_i (m)		T (s)	
	1	5.4	8	12
1 : 10	0.1	0.54	2.53	3.8
1 : 20	0.05	0.27	1.79	2.68
1 : 30	0.033	0.18	1.46	2.19
1 : 40	0.025	0.135	1.26	1.9

4.2 Composite porous structure with submerged plate

The composite structure is modelled with a 1:30 scale using Froude's similitude criteria. The investigations are conducted for different porosity of the structure and the submerged plate on varying the wave heights H and wave periods T. The composite breakwater consists of the fully-extended porous structure, submerged plate and bottom-standing porous structure, whose dimensions are listed in Table 3.

4.3 Experimental procedure

The experimental study is conducted for the composite bottom-standing porous structure, submerged porous plate,

Table 3 Structural dimensions of the model (m)

Structural parameters	Model dimensions		
	Width	Thickness	Height/Length
Bottom-standing stucture	0.72	0.15	0.25
Submerged plate	0.72	0.002	1.0
Fully extended structure	0.72	0.15	0.5

and fully-extended porous structure. The wave flume is calibrated for different water depths to obtain the incident wave heights for different combinations of wave height and wave period. The capacitance type wave probes are installed to measure the water surface elevation and the wave probes are calibrated every time before starting the experiment. The wave height is measured using three probe method as suggested by Isaacson (1991) to calculate the wave reflection. Three probes are installed before the model (in the seaward side) to measure the incident and reflected wave height. The spacing between the probes in the seaward side is adjusted to one-third of the wavelength to ensure accuracy of wave reflections (Goda and Syzuki, 1976; Isaacson, 1991). The transmitted wave heights are recorded from a probe which is placed at a distance L from the model towards the lee side. The list of experimental variables used in the present investigation is presented in Table 4 and the experimental set up for the composite breakwater is shown in Figure 3. The accuracy of the experiments is ensured by repeating the cases thrice under the same conditions.

4.4 Reflection transmission and dissipation coefficient

The wave reflection coefficient is obtained as the ratio of the reflected wave height and incident wave height represented as

$$K_r = \frac{H_r}{H_i} \tag{32}$$

The reflected wave height H_r are obtained by the three-probe method as proposed by Issacson (1991). The wave

Table 4 Experimental variables of composite breakwater

Variables	Expression	Parameter range
Wave period (s)	T	1.4, 1.6, 1.8, 2.0
Incident wave height (m)	H_i	0.06, 0.08, 0.10, 0.12, 0.14
Water depth (m)	h	0.45
Angle of wave attack	θ	0°
Incident wave steepness	H_i/gT^2	0.001 5 – 0.006 2

transmission coefficient is obtained as the ratio of the transmitted wave height and incident wave height given by

$$K_t = \frac{H_t}{H_i} \tag{33}$$

The dissipation coefficient is obtained by considering the energy balance condition as in Eq. (28b). In the present study, the experimental investigation is performed to validate the numerical results obtained using the eigenfunction expansion method.

5 Numerical results and discussions

The numerical investigation for the wave interaction

Figure 3 Experimental setup for composite breakwater in NITK wave flume

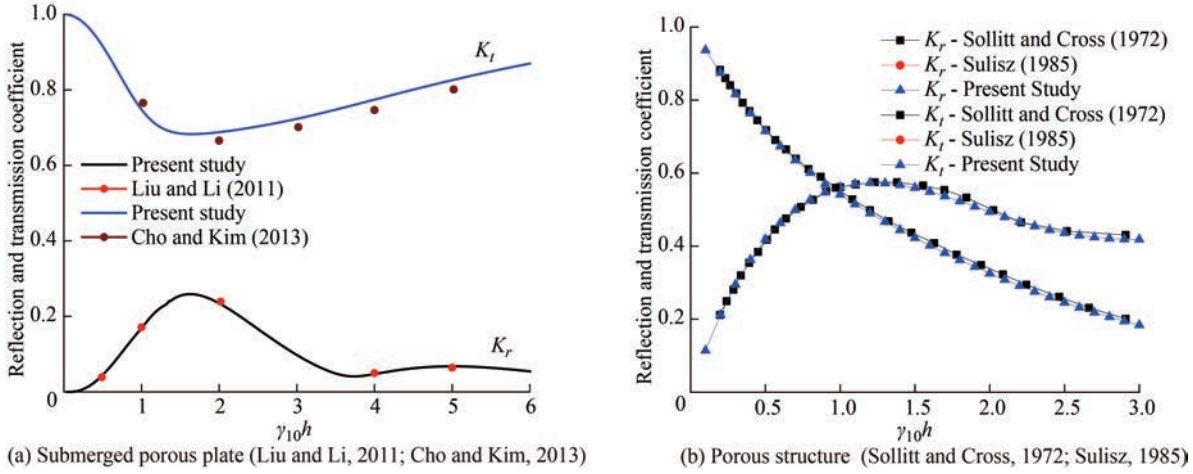

Figure 4 Comparative study of submerged porous plate and porous structure

with the combined bottom-standing porous structure, submerged porous plate and fully extended porous structure is conducted using the small amplitude wave theory. The analysis is performed to understand the effect of structural and geometrical parameters such as structural porosity, submergence depth of plate, angle of incidence and width of the porous structures on wave energy dissipation. The reflection coefficient K_r, transmission coefficient K_t and dissipation coefficient K_d are analysed. In addition, the wave force on the front $K^1_{fs_1}$ and back $K^1_{fs_2}$ of the bottom standing porous structure, wave force on the plate K_{fp}, wave force on the front $K^2_{fs_1}$ and back $K^2_{fs_2}$ of the fully extended porous structure are also analysed. The parameters such as density of the fluid $\rho = 1\,025\ \text{kg/m}^3$ and acceleration due to gravity $g = 9.8\ \text{m/s}^2$ are kept constant throughout the numerical modelling. The convergence study for the K_r and K_t due to the increasing number of evanescent modes M is performed and it is noted that, with the increasing number of evanescent mode $M \geqslant 10$ the convergence in the reflection and transmission coefficient is evident. In order to validate the numerical model developed using the eigenfunction expansion method, the comparative study with the results of the single submerged plate (Liu and Li, 2011; Cho and Kim, 2013) and submerged porous structure (Sollitt and Cross, 1972; Sulisz, 1985) is performed and discussed in detail. Further, the experimental investigation for the combined porous structure with submerged porous plate is perfomed and the results for the experimental study are compared with the numerical results as obtained using the eigenfunction expansion method.

5.1 Validation of numerical and experimental model

The comparative study of the numerical model is performed with the results of the submerged plate (Liu and Li, 2011; Cho and Kim, 2013) and submerged porous structure (Sollitt and Cross, 1972; Sulisz, 1985) in Figure 4. The comparative study for the submerged plate (Figure 4(a)) with Liu and Li (2011) and Cho and Kim (2013) shows that the numerical result obtained using the present approach coincide with the result available in the literature. The maximum value of the reflection coefficient is observed within $1.2 < \gamma_{10}h < 1.6$ and with the increase in the wavenumber the K_r decreases and approaches to minimum.

The wave transformation due to the rectangular porous structure with finite thickness is compared with Sollitt and Cross (1972) and Sulisz (1985) in Figure 4 (b) on comparing the K_r and K_t for $\varepsilon_s = 0.4$ and $f = 0.5$. The comparative study shows a good agreement of the numerical result with Sollitt and Cross (1972). The study shows that, the wave reflection coefficient increases within $0.01 < \gamma_{10}h < 1.5$ and thereafter decreases. On the other hand, the transmission coefficient decreases with the increase in $\gamma_{10}h$.

In Figure 5, the numerical investigation on the wave reflection and transmission coefficient performed for the composite porous structure with submerged plate is validated with the physical model study. The reflection coefficient K_r (Figure 5(a)) and transmission coefficient K_t (Figure 5(b)) are plotted against the non-dimensional wave number $\gamma_{10}h$ for varying plate porosity ε_2. It is observed that the data obtained using the experimental study follows the similar pattern with the numerical results within the range $0.6 < \gamma_{10}h < 1.2$. The variation of about 5%–10% in the hydrodynamic coefficients is noted on comparing the experimental and numerical result within $0.6 < \gamma_{10}h < 1.2$ for different plate porosity. The variation in the numerical and experimental result may be due to consideration of the fluid to be inviscid in the numercal investigation. Further, the friction and inertia present in the model setup are unknown during the experimental investigation, but they are incorporated with assumed values during the numerical analysis which may be one of the cause in the variation in the experimental and numerical studies. Additionally, the

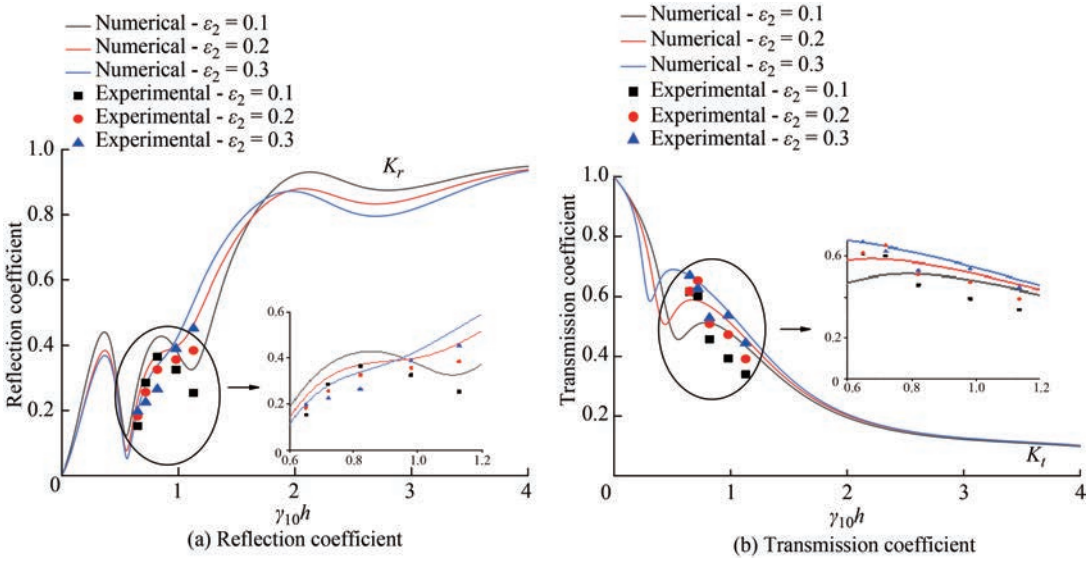

Figure 5 Comparative study of K_r and K_t for composite bottom-standing porous structure, submerged porous plate and fully-extended porous structure

numerical model is considered to be infinite, whereas the experimental wave tank is horizontally finite, which may potentially cause differences in the hydrodynamic coefficient values between the investigations.

5.2 Wave reflection, transmission and dissipation coefficient

The composite breakwater system's hydrodynamic performance is analyzed on studying the wave reflection, transmission and dissipation coefficients for different physical and geometrical parameters. The study performed on the wave scattering by the submerged structure enables us to understand the effectiveness of the composite breakwater system due to the action of high waves.

5.2.1 Effect of porosity of the fully-extended porous structure

Figure 6 shows the reflection K_r, transmission K_t and dissipation K_d coefficients against the non-dimensional wave number $\gamma_{10}h$ for different porosity of fully-extended porous structure ε_3 within $0.2 < \varepsilon_3 < 0.8$. In Figure 6(a), the reflection coefficient shows an oscillating pattern within $0.01 < \gamma_{10}h < 1.15$ and suddenly increases for all values of ε_3. The study noted that the value of K_r is higher for minimum porosity and is lower for maximum porosity. Further, the transmission coefficient decreases upto $\gamma_{10}h = 0.5$ and then increases within $0.5 < \gamma_{10}h < 1.0$ and thereafter K_t decreases with increase in $\gamma_{10}h$. The transmission coefficient of a fully-extended porous structure also increases as the porosity increases which may be due to the fact that, as the structure's porosity increases, more water can pass through the pore space, thus increasing the transmission coefficient and decreasing the reflection coefficient. The wave energy dissipation is noted higher when the porosity of the fully-extended structure is low (Figure 6(b)). This could be due to the damping of waves within the spaces between the porous structures, as the porosity decreases. The damping coefficient is noted minimum within $1.8 < \gamma_{10}h < 4.0$.

5.2.2 Effect of submergence depth of plate

The reflection K_r, transmission K_t and dissipation K_d coefficients (Figure 7) are plotted against the non-dimensional wave number $\gamma_{10}h$ for varying plate submergence depth h_1/h. In Figure 7(a), it is observed that the reflection coefficient shows an oscillating trend as $\gamma_{10}h$ increases for all values of plate submergence depth. It is noted that the reflection coefficient decreases as the plate submergence depth increases. The reflection coefficient K_r almost remains constant for $\gamma_{10}h > 4$ as plate submergence depth increases. Further, the transmission coefficient decreases up to $\gamma_{10}h = 1$ and then oscillates to a constant value as in the case of the reflection coefficient. The higher submergence depths result in a higher transmission coefficient. The higher transmission coefficient with the increase in submergence depth may be due to the free flow water above the porous plate, allowing more wave transmission and less reflection. The effectiveness of the porous structure is enhanced when the porous plate is kept at the water surface level, since the wave energy dissipation (Figure 7(b)) of the structure is higher when $h_1/h = 0$. The wave damping is noted to decrease with the increase in the submergence depth of the plate as most of the wave energy is concentrated at the free surface.

5.2.3 Effect of angle of incidence

In Figure 8, the refection K_r, transmission K_t and dissipation K_d coefficients are plotted against the angle of incidence θ for various values of porosity ε_3 of fully-extended porous structure. It is noted that for $\varepsilon_3 = 0.2$, the reflection

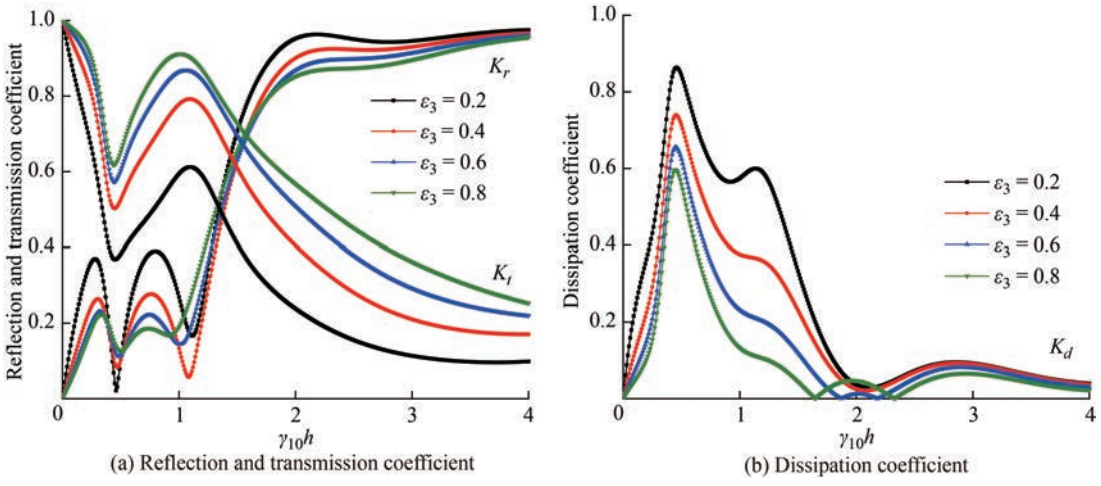

Figure 6 Variation in K_r, K_t and K_d versus $\gamma_{10}h$ for different values of porosity of fully extended porous structure ε_3 considering $\theta = 30°$ and $h_1/h = 0$

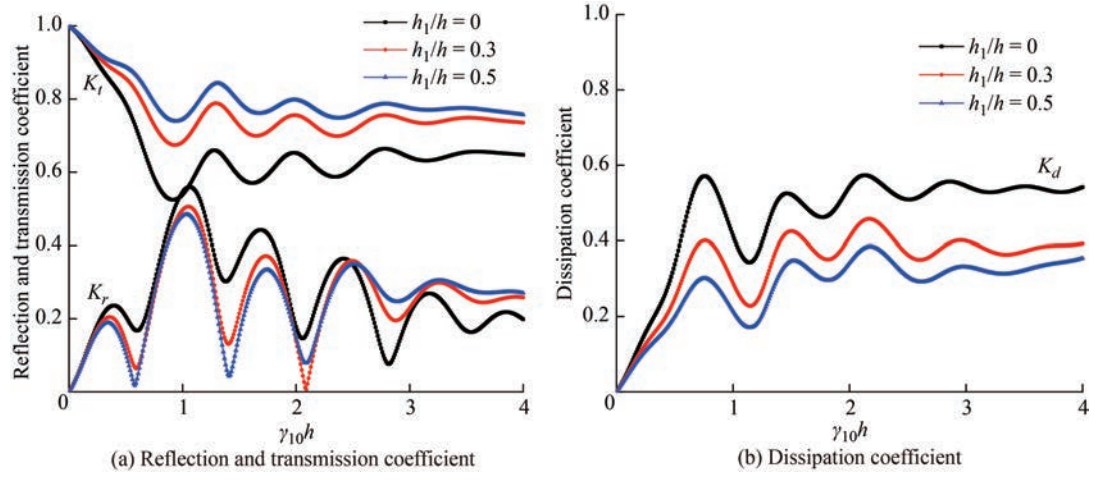

Figure 7 Variation in K_r, K_t and K_d versus $\gamma_{10}h$ for different values of plate submergence depth h_1/h considering $\theta = 30°$ and $\varepsilon_3 = 0.3$

coefficient decreases slightly up to $\theta = 38°$ and then increases for higher values of angle of incidence. Whereas for higher values of porosity of fully-extended porous structure, the value of K_r increases as the angle of incidence increases. The transmission coefficent (Figure 8(a)) is observed maximum for $\theta = 0°$ and for maximum porosi-

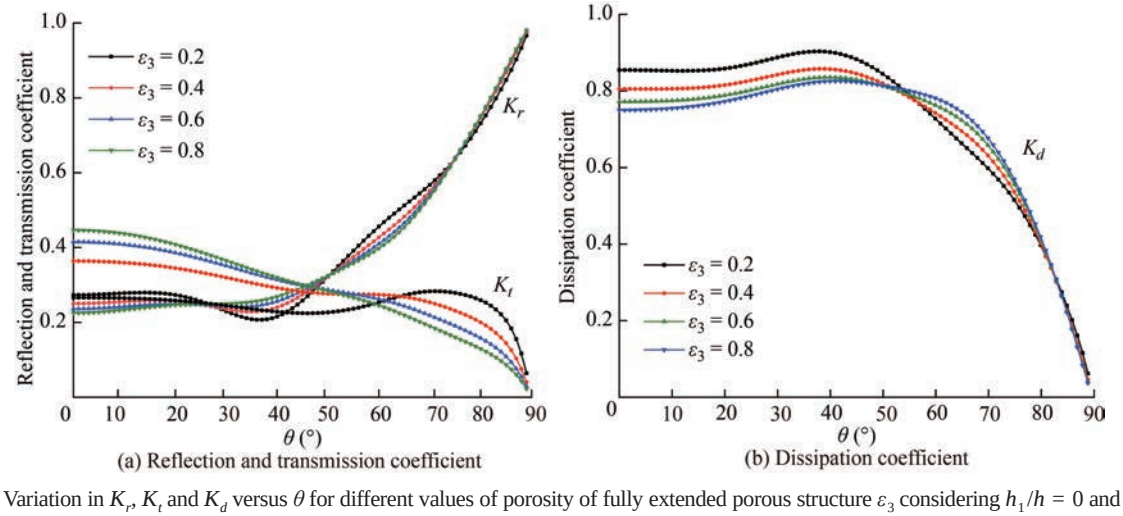

Figure 8 Variation in K_r, K_t and K_d versus θ for different values of porosity of fully extended porous structure ε_3 considering $h_1/h = 0$ and $\varepsilon_1 = 0.3$

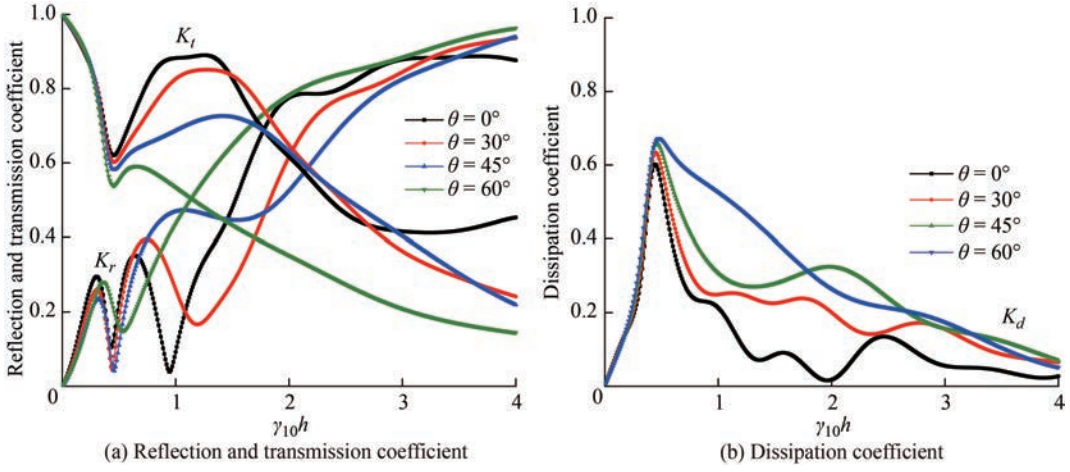

Figure 9 Variation in K_r, K_t and K_d versus $\gamma_{10}h$ for different values of angle of incidence θ considering $\varepsilon_1 = 0.3$, $h_1/h = 0$ and $\varepsilon_3 = 0.3$

ty of the fully-extended structure. The minimum wave reflection is observed in the range of $30° < \theta < 40°$ which can be considered as the critical angle. Thus, it can be concluded that the critical wave angle lies within $30° < \theta < 40°$, which will help in the design of coastal defence structures for minimum wave reflection. The transmission coefficient decreases as the angle of incidence increases for higher values of porosity. Whereas in case of $\varepsilon_3 = 0.2$, a slight increase in transmision coefficient is observed within $45° < \theta < 75°$ after which the value of K_t (Figure 8(a)) suddenly decreases. The wave energy dissiaption (Figure 8(b)) is observed higher for minimum porosity up to $\theta = 55°$ and thereafter K_d is higher for minimum porosity. It is observed that the dissipation coefficient increases up to $\theta = 55°$ and then there is a sudden drop in energy dissipation coefficient.

Figure 9 shows the reflection, transmission and dissipation coefficient against the non-dimensional wave number $\gamma_{10}h$ for different values of angle of incidence. It is observed that as the angle of incidence increases, the reflection coefficient (Figure 9(a)) increases while the transmission coefficient decreases. This could be due to the fact that as the angle of incidence increases, the wave is reflected more rather than passing through the porous structure, resulting in increased reflection and decreased transmission. Further, it is noted that the wave attenuation increases as the angle of incidence increases. The wave dissipation coefficient (Figure 9(b)) attains maximum value within $0.25 < \gamma_{10}h < 0.75$ and thereafter approach to minimum value with the increase in $\gamma_{10}h$. The higher wave energy dissipation is noted in the shallow water region and with the change in the angle of incidence the K_d is observed same within $0 < \gamma_{10}h < 0.5$.

5.2.4 Effect of plate length

The reflection K_r, transmission K_t and dissipation coefficients K_d (Figure 10) are plotted against the non-dimensional wave number $\gamma_{10}h$ for different values of plate length a/h. The reflection coefficient (Figure 10(a)) is oberved to increase as the plate length increases up to $\gamma_{10}h = 0.75$. Further, it is observed that the reflection coefficient is higher for $a/h = 3.0$ up to $\gamma_{10}h = 3$ and beyond $\gamma_{10}h = 3$, the value of K_r is higher for $a/h = 3.5$

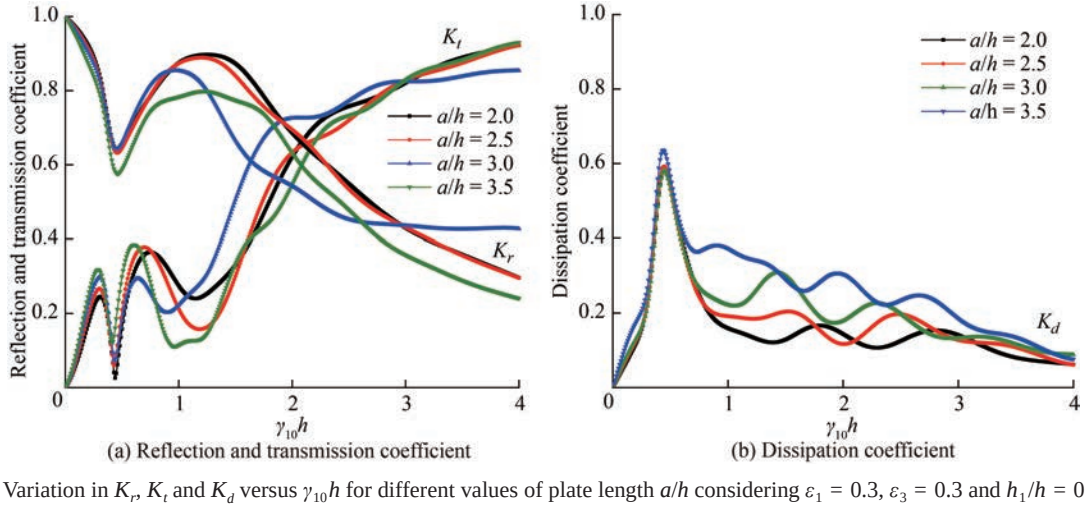

Figure 10 Variation in K_r, K_t and K_d versus $\gamma_{10}h$ for different values of plate length a/h considering $\varepsilon_1 = 0.3$, $\varepsilon_3 = 0.3$ and $h_1/h = 0$

(Figure 10(a)). The wave transmission is observed to reduce as the plate length increases. This may be due to the attenuation of more waves throughout the length of the plate as the plate length increases and hence reducing the transmision coefficient. The wave transmission coefficient is reduced to 0.25 from 1.0 as the plate length increases within $2.0 < a/h_1 < 3.5$. Thus as the plate length is increased, the energy dissipation coefficient increases, which could be due to increased wave-porous plate interaction. Further, the dissipation coefficient (Figure 10(b)) is noted to be same for all plate lenghts within $0.25 < \gamma_{10}h < 0.75$ and therafter an oscillating decreasing trend is noted for $\gamma_{10}h \geqslant 1.0$.

5.2.5 Effect of width of fully-extended porous structure

In Figure 11, the reflection, transmission and dissipation coefficient are plotted the against the width of the fully-extended porous structure w_2/h for different angle of incidence. The reflection coefficient (Figure 11(a)) shows an oscillating trend as the width of the fully-extended porous structure increases. In addition, the resonating crest and trough of the reflection coefficient are observed to be decreasing as the width of the fully-extended porous structure increases. It is noted that for normal angle of incidence $\theta = 0°$, the resonating trough of wave reflection coefficient reduces to 0.02 at $w_2/h = 1.2$. Further, as the width of the fully-extended porous structure increases, the resonating peak and trough increases. It is also observed that the transmission coefficient decreases as the width of the fully extended porous structure increases and the transmission coefficient reduces to 0.1 from 0.55 for $\theta = 60°$. The trend shows the increase in the reflection coefficient and decrease in the transmission coefficient as the angle of incidence increases. The decrease in reflection and transmission coefficients as the width of the fully extended porous structure increases could be due to the wave being damped within the structure, resulting in higher wave energy dissipation (Figure 11(b)). The energy dissipation coefficient shows oscillating trend with the increase in the width of the fully-extended porous structure for various angle of incidence.

5.2.6 Effect of distance between the porous structure and submerged plate

In Figure 12, the reflection, transmission and dissipation coefficient are plotted against the distance between the porous structure and the submerged plate L/h for different angle of incidence. In Figure 12(a), the reflection coefficient shows a resonating trend as the distance between the porous structure and the plate increases. At the resonating crests, the reflection coefficient decreases as the porosity of the fully-extended porous structure increases, while at the resonating troughs, the reflection coefficient increases as the porosity of the fully-extended porous structure increases. The constructive and destructive interferences of the waves cause the resonating patterns to appear. The transmission coefficient, on the other hand, appears to increase as the porosity of the fully extended porous structure increases, both at the resonating peaks and troughs. The resonating pattern could be caused by the waves being trapped in the space between the porous structures. On the other hand, the dissipation coefficient (Figure 12(b)) is observed more for minimum porosity of the fully-extended porous structure. In addition the dissipation coefficient shows maximum value within $0 < L/h < 0.5$ and $3.5 < L/h < 4.5$.

5.3 Wave force on the structure

The effect of the wave force on the submerged structure, floating plate and fully extended structure is investigated for different physical and geometrical parameters to analyse the effectiveness of the composite breakwater system.

5.3.1 Effect of porosity of fully-extended porous structure

In Figure 13, the wave force on front $K^1_{fs_1}$ and back $K^1_{fs_2}$ of the bottom-standing porous structure, wave force on the submerged plate K_{fp}, wave force on front $K^2_{fs_1}$ and back $K^2_{fs_2}$

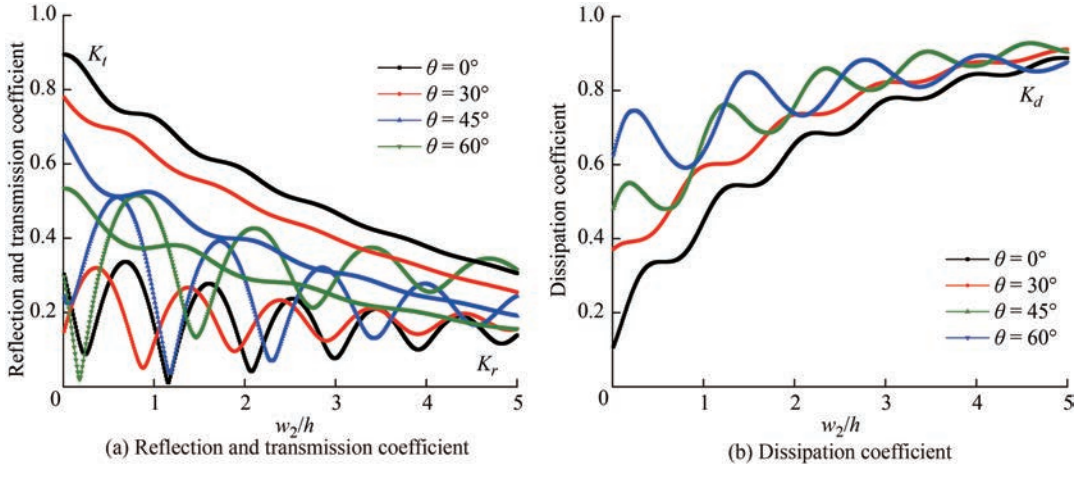

Figure 11 Variation in K_r, K_t and K_d versus w_2/h for different values of angle of incidence considering $\varepsilon_1 = 0.3$, $\varepsilon_3 = 0.3$ and $h_1/h = 0$

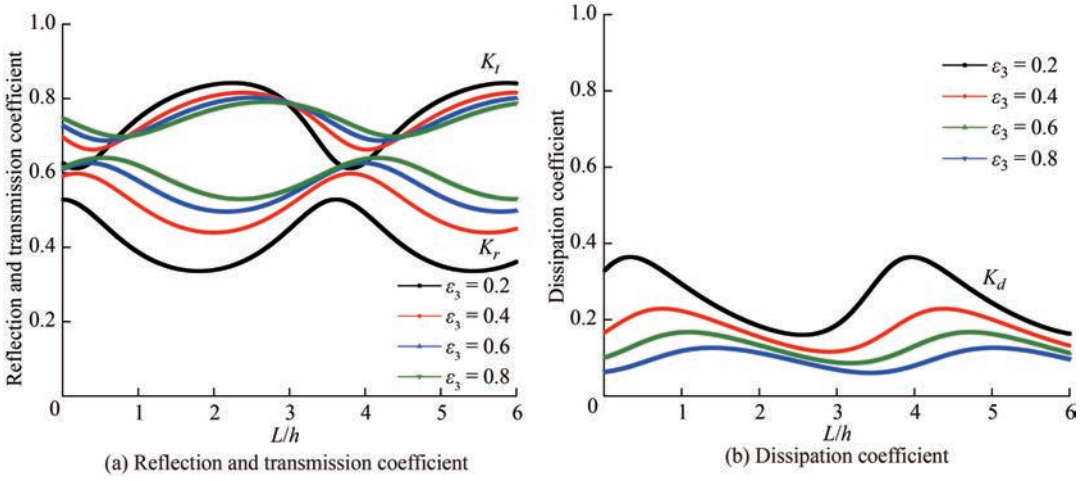

Figure 12 Variation in K_r, K_t and K_d versus L/h for different values of porosity of fully-extended porous structure considering $\theta = 30°$ and $h_1/h = 0$

of the fully-extended porous structure are plotted against the angle of incidence θ for different values of porosity ε_3 of fully-extended porous structure. The porosity of the bottom stanidng porous structure $\varepsilon_1 = 0.3$ and submerged porous plate $\varepsilon_2 = 0.1$ are kept constant. In Figure 13(a), it is observed that the wave force on the bottom standing porous structure has less effect due to the change in ε_3. But the slight variation suggests that when the porosity of fully-extended structure is lower then wave transmission will be less and the wave gets reflected and increases the force on bottom-standing structure. As the porosity of the fully-extended porous structure increases, the wave force on the submerged porous plate decreases (Figure 13(b)). Similarly, in Figure 13(c) as the porosity of the structure increases, the wave force on the front and back of the fully-extended porous structure decreases. This could be due to the fact that as the porosity of the full-extended porous structure increases, waves can easily pass through it, allowing for more transmission and reducing the wave force impact on the structure.

5.3.2 Effect of submergence depth of plate

Figure 14 presents the wave force on front $K^1_{fs_1}$ and back $K^1_{fs_2}$ of the bottom standing porous structure, wave force on the submerged plate K_{fp}, wave force on front $K^2_{fs_1}$ and back $K^2_{fs_2}$ of the fully extended porous structure plotted against the angle of incidence θ for different values of submergence depth of plate h_1/h. As the angle of incidence increases, the wave force on the front and back of the bottom-standing porous structure (Figure 14(a)) decreases. Further, as the plate submergence depth increases, the wave force on the front and back of the bottom-standing porous structure does not show much variation. In Figure 14(b), the wave force on the plate decreases as the angle of incidence increases. Similar to $K^1_{fs_1}$ and $K^1_{fs_2}$, the value of K_{fp} is maximum for $\theta = 0°$. Figure 14(c) shows that the wave force on the front and back of the fully extended porous structure also decreases as the angle of incidence increases. The wave force on the front and back of the fully-extended porous structure does not differ significantly as the plate submergence depth increases. When compared to porous plates and bottom-standing porous structures, it is seen that the wave forces acting on fully-extended porous structures are substantially lower. This might be because the porous plate and the bottom-standing porous structure help to dissipate wave energy, which further reduces the impact of waves on the fully-extended porous structure.

5.3.3 Effect of width of fully-extended porous structure

In Figure 15, the wave force on front $K^1_{fs_1}$ and back $K^1_{fs_2}$ of the bottom-standing porous structure, wave force on the submerged plate K_{fp}, wave force on front $K^2_{fs_1}$ and back $K^2_{fs_2}$ of the fully-extended porous structure are plotted against the width of the fully-extended porous structures w_2/h for different values of angle of incidence θ.

In Figure 15(a), it is noted that the wave force on the front of the bottom-standing porous structure increases as the width of the fully-extended porous structure increases for $\theta = 0°$. Then for higher values of angle of incidence, the value of $K^1_{fs_1}$ increases and decreases within $0.01 < w_2/h < 1$ and afterwards it shows a gradual increase for higher width of fully-extended porous structure. The wave force on the back of the bottom-standing porous structure has a wavy nature within $0.01 < w_2/h < 3$. Beyond that, the value of $K^1_{fs_2}$ remains constant. In Figure 15(b), the wave force on the plate decreases as the width of the fully-extended porous structure increases for $\theta = 0°$ and for greater values of θ, the value of K_{fp} increases and decreases within $0.01 < w_2/h < 1$ and then decreases eventually. The wave force on the front and back of the fully extended porous structure shows a similar trend (Figure 15(c)). It is also noted that within $0.01 < w_2/h < 1$, the wave force is higher for higher angle of incidence whereas for $w_2/h > 1.0$,

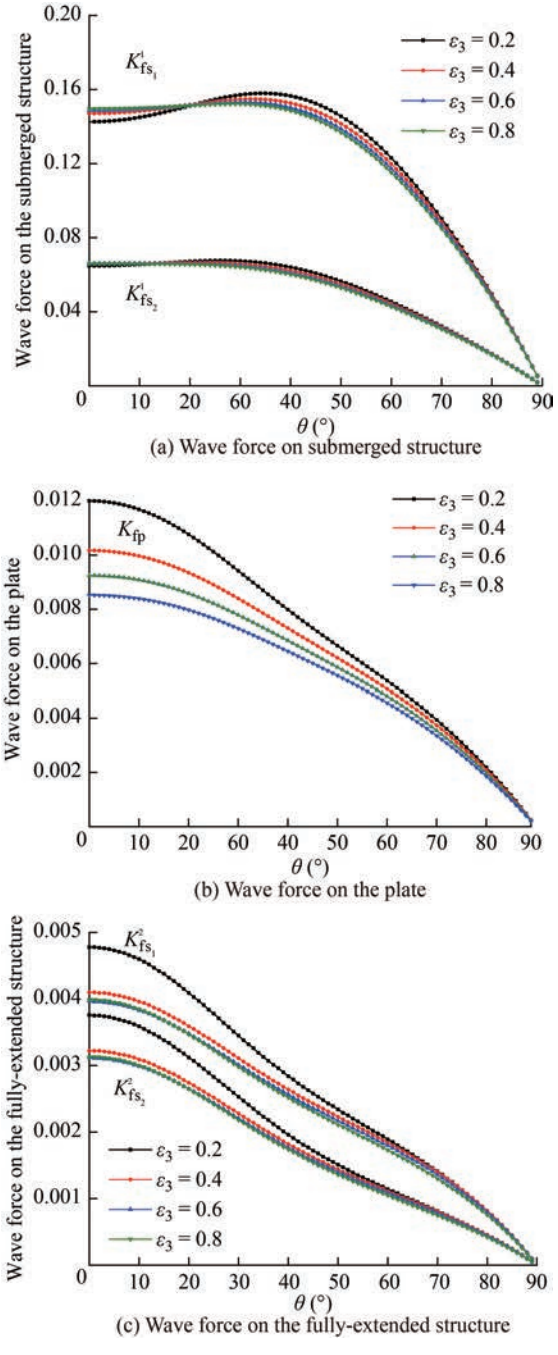

Figure 13 Variation in wave force on submerged structure, plate and fully-extended structure versus θ for different values of porosity ε_3 considering $\varepsilon_1 = 0.3$ and $h_1/h = 0$

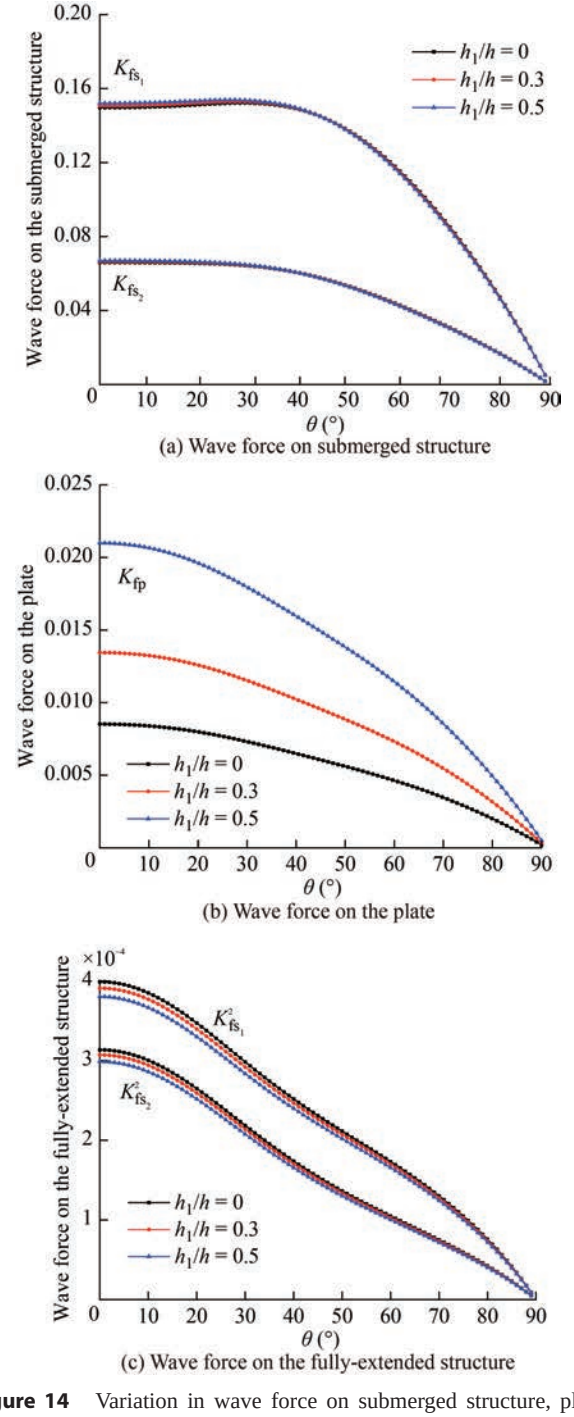

Figure 14 Variation in wave force on submerged structure, plate and fully-extended structure versus θ for different values of plate submergence depth h_1/h considering $\varepsilon_1 = 0.3$ and $\varepsilon_3 = 0.3$

the wave force is less for higher angle of incidence.

5.3.4 Effect of distance between the porous structure and submerged plate

Figure 16 shows the wave force on front $K^1_{fs_1}$ and back $K^1_{fs_2}$ of the bottom standing porous structure, wave force on the submerged porous plate K_{fp}, wave force on front $K^2_{fs_1}$ and back $K^2_{fs_2}$ of the fully extended porous structure against the distance between the porous structure and submerged plate L/h for different values of angle of incidence θ.

In Figure 16(a), the wave force of the front and back of the bottom stadning structure shows a resonating pattern as the distance between the porous structure and the submerged plate increases. It is also observed that the wave force on the bottom-standing porous structure reduces with increase in angle of incidence. In Figure 16(b), the wave force on the sumerged porous plate is observed to

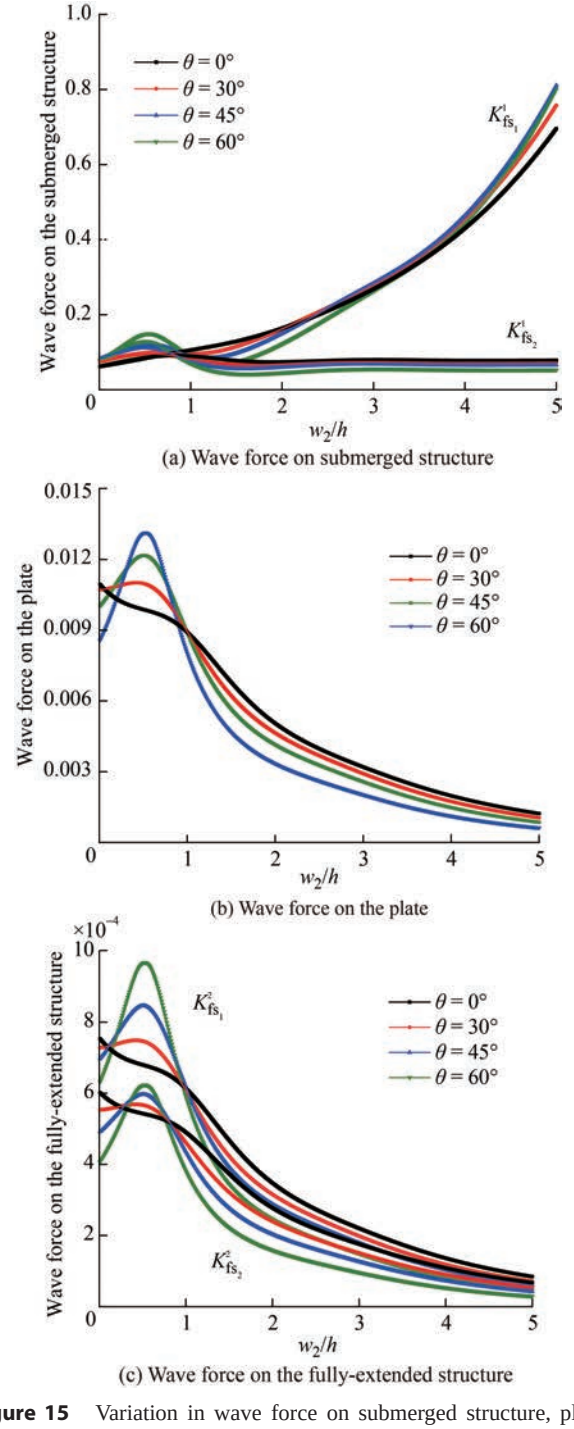

Figure 15 Variation in wave force on submerged structure, plate and fully-extended structure versus w_2/h for different values of angle of incidence θ considering $\varepsilon_1 = 0.3$ and $h_1/h = 0$

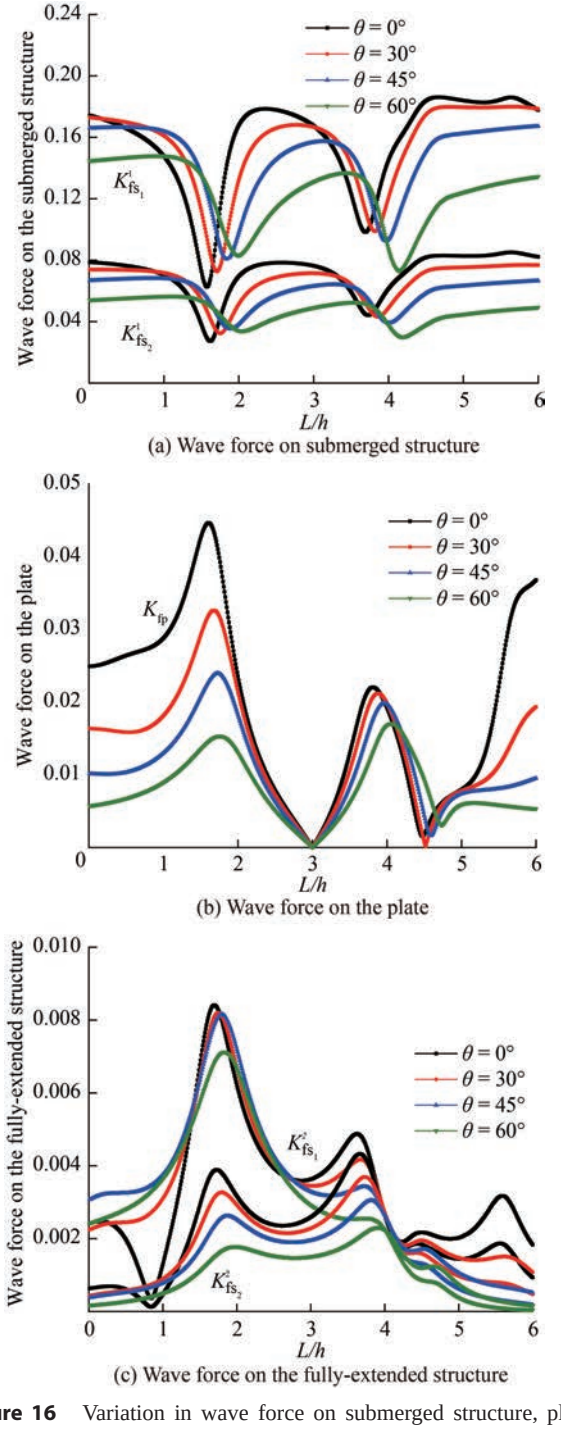

Figure 16 Variation in wave force on submerged structure, plate and fully-extended structure versus L/h for different values of angle of incidence θ considering $\varepsilon_1 = 0.3$ and $h_1/h = 0$

increase to a maximum value at $L/h = 1.5$ and then decreases to almost zero for all values of angle of incidence. Thereafter, it again increases and decreases to almost zero at $L/h = 4.5$. This may be due to the wave attenuation in the confined region between the porous structure and the submerged plate. In Figure 16(c), the wave force on the front of the fully extended porous structure shows a maximum value at $L/h = 0.75$ and then decreases as L/h increases. The wave force on the back of the fully-extended porous structure also shows an oscillating trend with increase in L/h. The resonating trend in the wave forces could be due to the trapping of waves in the free space between the submerged plate and porous structure.

6 Conclusions

The wave damping due to the combination of bottom-standing porous structure, submerged horizontal porous plate and fully-extended porous structure is studied using the eigen function expansion method and orthogonal mode-coupling relation. The hydrodynamic coefficients obtained using the numerical investigation are validated using the experimental results. The effect of various physical and geometrical parameters on the wave force on the structure are also analysed for the combined porous structure with the submerged plate. The conclusions drawn from the present study are as follows:

1) The performance of the composite breakwater system is observed better when the plate is on the water surface and the energy damping is maximum at plate submergence depth close to the free-surface. The resonating trend in reflection and transmission is observed for the composite breakwater system which may be the trapping of waves in the confined regions in the porous structure, and may be due to the formation of standing waves in the gaps between the porous structures.

2) The wave reflection is observed higher for the submerged plate at the free surface and the porus structure with less porosity and the transmission coefficient is observed to be low and also the wave energy dissipation high for larger plate lengths.

3) The hydrodynamic coefficients show an oscillating pattern as the distance between the porous structure and the submerged plate L/h varies. So, a suitable value of L/h should be chosen where the transmission coefficient is low and energy dissipation is higher.

4) The increase in width of the fully-extended structure w_2/h improves the performance characteristics of the proposed composite breakwater system. Further, it is observed that when $w_2/h < 1.0$, the wave force on the structure is higher. So, it is better to choose $w_2/h > 1$ for the design purpose.

5) The wave force on the structure and wave transmission is higher at lower angle of incidence whereas the reflection coefficient is minimum at $\theta = 0°$. Further, the wave force on the fully-extended structure is reduced significantly with the inclusion of the submerged porous plate and bottom-standing structure for varius submergence depth of the plate.

Nomenclature

b	Distance between the porous structure
f	Linearized friction factor
g	Accelaration due to gravity
h	Water depth
h_1	Submergence depth of plate and bottom-standing porous structure
i	Imaginary number
k_{jn}	Wave number in x-direction
K_r	Reflection coefficient
K_t	Transmission coefficient
K_d	Dissipation coefficient
$K^1_{\mathrm{fs}_1}$	Wave force on the front of the bottom-standing porous structure
$K^1_{\mathrm{fs}_2}$	Wave force on the back of the bottom-standing porous structure
K_{fp}	Wave force on submerged porous pate
$K^2_{\mathrm{fs}_1}$	Wave force on the front of the fully-extended porous structure
$K^2_{\mathrm{fs}_2}$	Wave force on the back of the fully-extended porous structure
l	Wave number in z-direction
L	Distance between the plate and porous structures
s	Inertial effect of the porous medium
w_1	Width of the bottom-standing porous structure
w_2	Width of the fully-extended porous structure
γ_{jn}	Wave number in y-direction
ε_j	The porosity of each layer
θ	Angle of incidence
η_j	Free surface wave elevation
ρ	Density of water
ω	Wave frequency
ϕ	Velocity potential

Acknowledgement

The authors acknowledge Science and Engineering Research Board (SERB), Department of Science & Technology (DST), Government of India for supporting financially under the research Grant No. CRG/2018/004184 and Ministry of Ports, Shipping and Waterways, Government of India through the research Grant No. DW/01013(13)/2/2021.

Competing interest D. Karmakar is an editorial board member for the Journal of Marine Science and Application and was not involved in the editorial review, or the decision to publish this article. All authors declare that there are no other competing interests.

References

Arunachalam VM (1982) Experimental studies on a perforated horizontal floating plate breakwater. Ocean Engineering 9(1): 35-45. https://doi.org/10.1016/0029-8018(82)90043-9

Bennett GS, McIver P, Smallman JV (1992) A mathematical model of a slotted wavescreen breakwater. Coastal Engineering 18(3-4): 231-249. https://doi.org/10.1016/0378-3839(92)90021-L

Cho IH, Kim MH (2013) Transmission of oblique incident waves by a submerged horizontal porous plate. Ocean Engineering 61: 56-65. https://doi.org/10.1016/j.oceaneng.2012.12.044

Cho IH, Koh HJ, Kim JR, Kim MH (2013) Wave scattering by dual submerged horizontal porous plates. Ocean Engineering 73: 149-158. https://doi.org/10.1016/j.oceaneng.2013.08.008

Dalrymple A, Losada A, Martin PA (1991) Reflection and transmission from porous structure under oblique wave attack. Journal of Fluid Mechanics 224: 625-644. https://doi.org/10.1017/S0022112091001908

Das S, Bora SN (2014) Reflection of oblique ocean water waves by a vertical rectangular porous structure placed on an elevated horizontal bottom. Ocean Engineering 82: 135-143. https://doi.org/10.1016/j.oceaneng.2014.02.035

Dattatri J, Shankar NJ, Raman H (1978) Performance characteristics of submerged breakwaters. Coastal Engineering 130: 2153-2171. https://doi.org/10.1061/9780872621909.132

Dick TM, Brebner A (1968) Solid and permeable submerged breakwaters. Coastal Engineering 72: 1141-1158. https://doi.org/10.1061/9780872620131.072

Goda Y, Suzuki Y (1976) Estimation of incident and reflected waves in random wave experiments. Proceedings of 15th Costal Engineering Conference (ASCE), Honolulu, 828-845. https://doi.org/10.1061/9780872620834.048

Huang LH, Chao HI (1992) Reflection and transmission of water wave by porous breakwater. Journal of Waterway, Port, Coastal and Ocean Engineering 118: 437-452. https://doi.org/10.1061/(ASCE)0733-950X(1992)118:5(437)

Isaacson M (1991) Measurement of regular wave reflection. Journal of Waterway, Port, Coastal, Ocean Engineering 117: 553-569. https://doi.org/10.1061/(ASCE)0733-950X(1991)117:6(553)

Koley S, Behera H, Sahoo T (2015) Interaction of gravity waves with bottom standing submerged structures having perforated outer-layer placed on a sloping bed. Applied Ocean Research 52: 245-260. https://doi.org/10.1016/j.apor.2015.06.003

Li AJ, Liu Y, Fang H (2021) Novel analytical solutions without finding complex roots for oblique wave scattering by submerged porous/perforated structures. Applied Ocean Research 112: 102685. https://doi.org/10.1016/j.apor.2021.102685

Liu Y, Li Y (2011) An alternative analytical solution for water-wave motion over a submerged horizontal porous plate. Journal of Engineering Mechanics 69: 385-400. https://doi.org/10.1007/s10665-010-9406-8

Losada IJ, Dalrymple RA, Losada MA (1991) Water waves on rown breakwaters. Journal of Waterway, Port, Coastal and Ocean Engineering 119(4): 367-380. https://doi.org/10.1061/(ASCE)0733-950X(1993)119:4(367)

Losada IJ, Losada MA, Martin FL (1995) Experimental study of wave induced flow in a porous structure. Coastal Engineering 26: 77-98. https://doi.org/10.1016/0378-3839(95)00013-5

Losada IJ, Silva R, Losada MA (1996) 3-D non-breaking regular wave interaction with submerged breakwaters. Coastal Engineering 28: 229-248. https://doi.org/10.1016/0378-3839(96)00019-1

Madsen (1983) Wave reflection from a vertical permeable wave absorber. Coastal Engineering 7: 381-396. https://doi.org/10.1016/0378-3839(83)90005-4

Mohapatra SC, Sahoo T, Guedes Soares C (2018) Surface gravity wave interaction with a submerged horizontal flexible porous plate. Applied Ocean Research 78: 61-74. https://doi.org/10.1016/j.apor.2018.06.002

Neelamani S, Gayathri T (2006) Wave interaction with twin plate wave barrier. Ocean Engineering 33(3-4): 495-516. https://doi.org/10.1016/j.oceaneng.2005.03.009

Neelamani S, Reddy MS (1992) Wave transmission and reflection characteristics of a rigid surface and submerged horizontal plate. Ocean Engineering 19(4): 327-341. https://doi.org/10.1016/0029-8018(92)90033-Z

Patil SB, Karmakar D (2022) Hydrodynamic analysis of floating tunnel with submerged rubble mound breakwater. Ocean Engineering 264: 112460. https://doi.org/10.1016/j.oceaneng.2022.112460

Sollitt CK, Cross RH (1972) Wave transmission through permeable breakwaters. Coastal Engineering 103: 1827-1846. https://doi.org/10.9753/icce.v13.99

Somervell LT, Thampi SG, Shashikala AP (2018) Estimation of friction coefficient of double walled permeable vertical breakwater. Ocean Engineering 156: 25-37. https://doi.org/10.1016/j.oceaneng.2018.02.050

Sulisz W (1985) Wave reflection and transmission at permeable breakwaters of arbitrary cross-section. Coastal Engineering 9: 371-386. https://doi.org/10.1016/0378-3839(85)90018-3

Ting CL, Lin MC, Cheng CY (2004) Porosity effects on non-breaking surface waves over permeable submerged breakwaters. Coastal Engineering 50: 213-224. https://doi.org/10.1016/j.coastaleng.2003.10.003

Twu SW, Chieu CC (2000) A highly wave dissipation offshore breakwater. Ocean Engineering 27: 315-330. https://doi.org/10.1016/S0029-8018(99)00002-5

Twu SW, Liu CC, Hsu WH (2002) Wave damping characteristics of deeply submerged breakwaters. Journal of Waterway, Port, Coastal and Ocean Engineering 127: 97-105. https://doi.org/10.1061/(ASCE)0733-950X(2001)127:2(97)

Venkateswarlu V, Karmakar D (2020) Significance of seabed characteristics on wave transformation in the presence of stratified porous block. Coastal Engineering Journal 62(1): 1-22. https://doi.org/10.1080/21664250.2019.1676366

Venkateswarlu V, Karmakar D (2021) Numerical investigation on the wave dissipating performance due to multiple porous structures. ISH Journal of Hydraulic Engineering 27(S1): 202-219. https://doi.org/10.1080/09715010.2019.1615393

Wang HY, Sun ZC (2010) Experimental study of a porous floating breakwater. Ocean Engineering 37: 520-527. https://doi.org/10.1016/j.oceaneng.2009.12.005

Xie JJ (2022) Long wave reflection by an array of submerged trapezoidal breakwaters on a sloping seabed. Ocean Engineering 252: 111138. https://doi.org/10.1016/j.oceaneng.2022.111138

Yang Z, Yong L, Huajun LI, Anteng C (2017) Oblique wave motion over multiple submerged porous bars near a vertical wall. Journal of Ocean University China 16(4): 568-574. https://doi.org/10.1007/s11802-017-3333-5

Zhu S, Chwang AT (2001) Analytical study of porous wave absorber. Journal of Engineering Mechanics 127: 326-332. https://doi.org/10.1061/(ASCE)0733-9399(2001)127:4(326)